ACS APPLIED MATERIALS & INTERFACES

Research Article

www.acsami.org

Cobalt Oxide (CoO_x) as an Efficient Hole-Extracting Layer for High-Performance Inverted Planar Perovskite Solar Cells

Ahmed Esmail Shalan,[†] Tomoya Oshikiri,[†] Sudhakar Narra,[‡] Mahmoud M. Elshanawany,[‡] Kosei Ueno,[†] Hui-Ping Wu,[‡] Keisuke Nakamura,[†] Xu Shi,[†] Eric Wei-Guang Diau,*[,‡] and Hiroaki Misawa*[,†,‡]

[†]Research Institute for Electronic Science, Hokkaido University, N21, W10, Kita-ku, 001-0021, Sapporo, Japan

[‡]Department of Applied Chemistry & Institute of Molecular Science, National Chiao Tung University, 1001 Ta Hsueh Road, Hsinchu 30010, Taiwan

Supporting Information

ABSTRACT: CoO_x is a promising hole-extracting layer (HEL) for inverted planar perovskite solar cells with device configuration ITO/CoO_x/$CH_3NH_3PbI_3$/PCBM/Ag. The devices fabricated according to a simple solution procedure showed the best photovoltaic performance attaining power conversion efficiency (PCE) of 14.5% under AM 1.5 G 1 sun irradiation, which is significantly superior to those of materials fabricated with a traditional HEL such as PEDOT:PSS (12.2%), NiO_x (10.2%), and CuO_x (9.4%) under the same experimental conditions. We characterized the chemical compositions with XPS, crystal structures with XRD, and film morphology with SEM/AFM techniques. Photoluminescence (PL) spectra and the corresponding PL decays for perovskite deposited on varied HEL films were recorded to obtain the hole-extracting characteristics, for which the hole-extracting times show the order CoO_x (2.8 ns) < PEDOT:PSS (17.5 ns) < NiO_x (22.8 ns) < CuO_x (208.5 ns), consistent with the trend of their photovoltaic performances. The reproducibility and enduring stability of those devices were examined to show the outstanding long-term stability of the devices made of metal oxide HEL, for which the CoO_x device retained PCE ≈ 12% for over 1000 h.

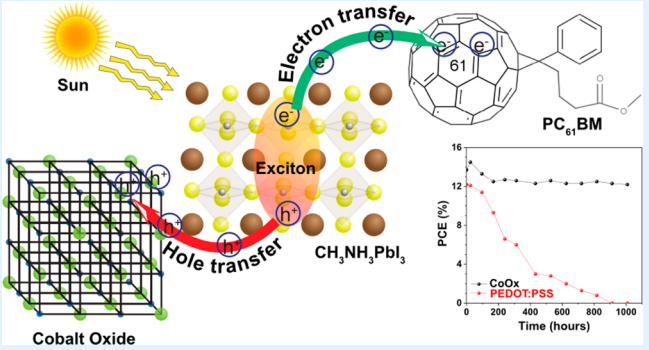

KEYWORDS: *cobalt oxide, hole-extraction layer, perovskite solar cell, photoluminescence, photovoltaic devices*

INTRODUCTION

Perovskite solar cells (PSC) based on organometallic trihalide perovskite materials ($CH_3NH_3PbI_3$, denoted as $MAPbI_3$) have attracted enormous research interest for solar-cell applications[1−3] owing to their many intriguing optical and electronic features, such as large absorption coefficient,[4] large charge-carrier mobility,[5,6] long carrier-recombination lifetime, and unique defect physics.[7] As a result, the efficiency of power conversion (PCE) of PSC quickly improved from 3.8%[8] to a certified value of 22.1% through developing the composition engineering,[9] interface engineering,[10,11] and processing methods.[12] Interest is growing in the inverted planar heterojunction (PHJ) PSC with the device configuration ITO/poly(3,4-ethylenedioxythiophene):polystyrenesulfonate (PEDOT:PSS)/$MAPbI_3$/[6,6]-phenyl-C_{61}-butanoic acid methyl ester (PCBM)/cathode, because the devices can be fabricated under low-temperature conditions with small hysteresis.[13,14] Accordingly, inverted PHJ devices using PEDOT:PSS as the hole-extracting layer (HEL) were reported to have PCE over 18% with a small active area[15,16] and a certified PCE 15% with a larger size (1 cm^2).[17]

With PCBM as an electron-extracting layer (EEL), PEDOT:PSS and its derivatives have been much used as HEL for inverted PHJ PSC.[18] As the open-circuit voltage (V_{OC}) is small and the hydrophilic and acidic nature of PEDOT:PSS deteriorate the device stability, varied types of inorganic semiconductors have been developed. For example, V_2O_3,[19−21] Mg-doped NiO_x ($Ni_xMg_{1-x}O$),[22] NiO_x,[17,23] Cu-doped NiO (Cu@NiO),[24] CuO_x,[25,26] and CuSCN[27] have been reported, but the devices made of those HELs performed poorly.[28] One reason for the poor performance is the thickness of the HEL, which was difficult to control within a few nanometers to avoid a large series resistance.[29] Furthermore, such an ultrathin layer could suffer from an ineffective surface coverage on a transparent conductive oxide substrate, as well as an insufficient surface roughness to deposit the $MAPbI_3$ layer with uniform morphology.[30] Among those inorganic semiconductors, NiO_x was one successful example acting as an HEL for inverted PHJ PSC with a satisfactory device performance.[31]

Received: August 27, 2016
Accepted: November 17, 2016
Published: November 17, 2016

DOI: 10.1021/acsami.6b10803
ACS Appl. Mater. Interfaces 2016, 8, 33592−33600

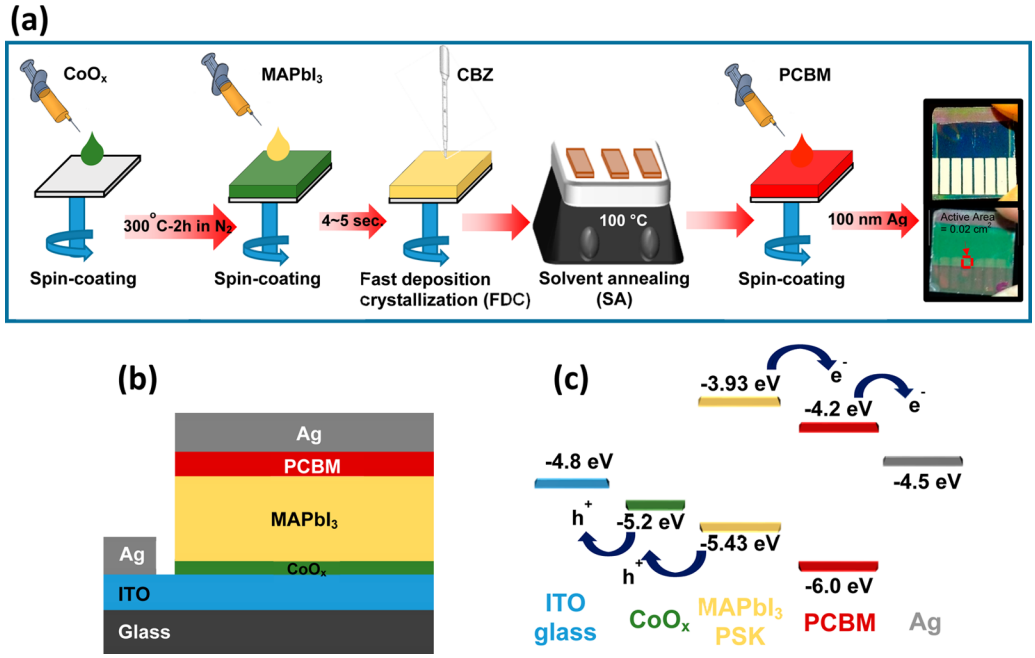

Figure 1. Schematic diagrams of (a) preparation of an inverted planar perovskite solar cell, (b) device configuration glass/ITO/CoO_x/$CH_3NH_3PbI_3$ perovskite/PCBM/Ag, and (c) the corresponding potential energy levels for each layer component. The potential energy levels for each component were cited in refs 27 and 57−59.

In the present work, we present the first demonstration of use of CoO_x as an efficient HEL for PSC applications: The ultrathin CoO_x film was prepared on an ITO substrate via spin-coating of the cobalt acetate tetrahydrate precursor solution to exhibit an effective surface coverage and great transparency in the visible region. The composition, crystallinity, morphology, and surface roughness of the CoO_x films were characterized via XPS, XRD, SEM, and AFM techniques, respectively. Our results show that uniform and flawless CoO_x films can be produced to avoid the charge recombination caused by the poor surface coverage of the film and that the film surface can be prepared with sufficient roughness to deposit uniform and well-packed perovskite nanocrystals with great hole-extraction capability. As a result, the inverted PHJ PSC devices made of the CoO_x film as an efficient HEL exhibit the best PCE, 14.5%, which outperforms those with the HEL made of PEDOT:PSS (12.2%), NiO_x (10.2%), and CuO_x (9.4%). Photoluminescence (PL) spectra and transient PL decays of perovskite deposited on varied HEL films were recorded; the results show the hole-extraction times (τ_h) with order $\tau_h(CoO_x) < \tau_h(PEDOT:PSS) < \tau_h(NiO_x) < \tau_h(CuO_x)$; this order is consistent with the trend of their photovoltaic performances, indicating the superior hole-extracting characteristic of the CoO_x film as an efficient HEL responsible for the high-performance inverted planar perovskite solar cells reported herein.

RESULTS AND DISCUSSION

Figure 1a presents a schematic diagram step by step of the preparation to fabricate our CoO_x device; the details are given in the Experimental Section. The right side of the scheme shows photographs of our device viewed from both sides. Figure 1b illustrates the side-view structure of a device with configuration glass/ITO/CoO_x/$MAPbI_3$/PCBM/Ag. The $MAPbI_3$ layer was deposited on the ITO/CoO_x substrate in one step through a fast deposition crystallization (FDC) in combination with solvent annealing (SA) reported elsewhere.[32,33] Following the deposition of the $MAPbI_3$ layer, a PCBM EEL was deposited with spin-coating.[34] The cells were completed with deposition of Ag back contacts via thermal evaporation in a vacuum chamber. Figure 1c shows the potential energy levels for each component of the device and the possible charge propagation paths for both photogenerated carriers, electrons (e^-) and holes (h^+), i.e., the dissociated charge carriers (e^- and h^+) in the $MAPbI_3$ layer can be extracted and transferred to the PCBM and CoO_x layers, respectively, further propagating toward each electrode. The energy level of the valence band of CoO_x is located at −5.2 eV,[35] which is above that of $MAPbI_3$ (−5.43 eV),[36,37] so that a suitable (quasi-)ohmic contact was achieved at the interface.

To confirm the crystal structures of the CoO_x film and other components, we undertook XRD analysis; the results are shown in Figure S1a. Besides the signals originating from the ITO substrate, the other diffraction line at ∼42° is indexed as the (200) facet of the standard rock-salt cubic CoO_x[38] (Powder Diffraction File (PDF) Nos. 9-402 and 9-418, International Centre for Diffraction Data (ICDD), 1971). After we carefully checked and characterized the obtained CoO phases and patterns, we confirmed that only the CoO diffraction peak at ∼42° is observed. The previous studies[38] claimed that at low oxygen flow rate and low temperature (100 sccm and 350−400 °C) only the CoO (200) reflection ($2\theta \approx 42.7°$) was observed and the other phases of other chemical valence of cobalt like Co_3O_4 (111) and (400) lines were hardly observable. That study is relevant our work because we have annealed our materials under nitrogen atmosphere with very low oxygen flow rate and at low temperature.[38] Figure S1a also shows the XRD characteristics of NiO_x and CuO_x. The obtained diffraction peaks of the HEL metal oxides of NiO_x and CuO_x are matched and correlated with the obtained phases in previous studies[39−41] (PDF No. 4-835, ICDD, 1993). Furthermore, the XRD patterns of the $CH_3NH_3PbI_3$films on the ITO substrate shown in Figure S1a confirm that the perovskite

DOI: 10.1021/acsami.6b10803
ACS Appl. Mater. Interfaces 2016, 8, 33592−33600

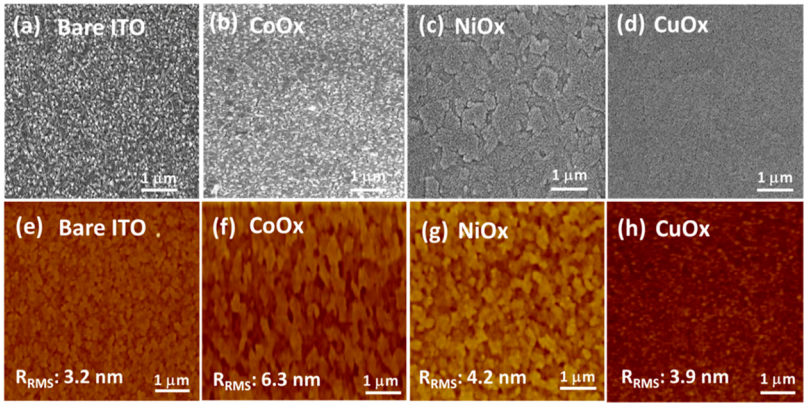

Figure 2. SEM images of (a) bare ITO, (b) CoO_x, (c) NiO_x, and (d) CuO_x and AFM images of (e) bare ITO, (f) CoO_x, (g) NiO_x, and (h) CuO_x.

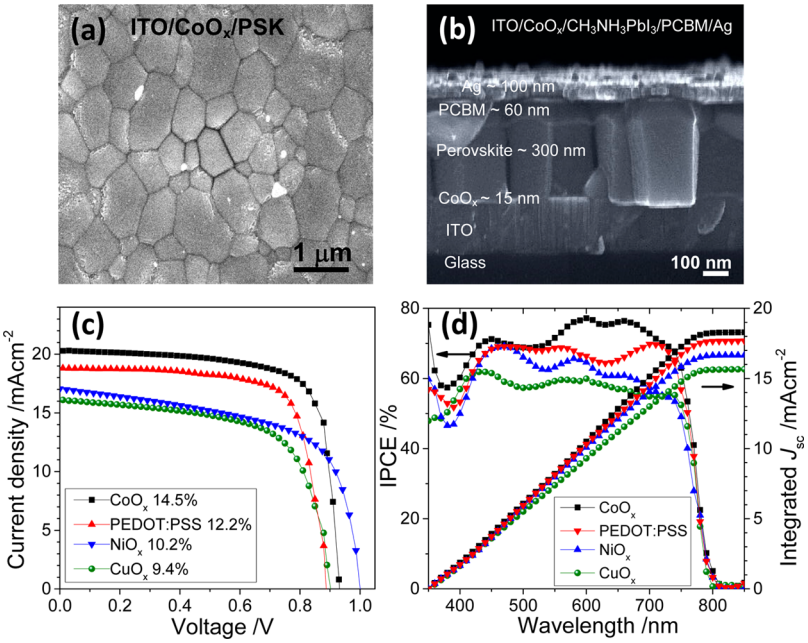

Figure 3. (a) Top-view SEM image of perovskite crystals deposited on CoO_x/ITO substrate. (b) Cross-sectional SEM image of CoO_x–based device. (c) Current–voltage curves and (d) IPCE and integrated current densities of CoO_x, PEDOT:PSS, NiO_x, and CuO_x devices as hole-extraction layers (HEL) as indicated.

crystals belong to the tetragonal phase; all diffraction signals are assigned according to data published elsewhere[42] and according to the Inorganic Crystal Structure Database entry code number 250739. No other impurity signal was detected, indicating that the produced $MAPbI_3$ crystal structures were highly pure with satisfactory crystallinity. For further confirmation, the XRD spectra of the perovskite layer deposited on the different HELs with the same conditions used in the photovoltaic devices were provided and shown in Figure S1b. The results confirm that the crystallinity of the perovskite layer is in the order of PSK/CoO_x > PSK/NiO_x > PSK/CuO_x which is in agreement with the sequence of the photovoltaic devices performances. Additional characteristics for the formation of the metal oxide films, CoO_x, NiO_x, and CuO_x, were derived from X-ray photoelectron spectra (XPS), wide and narrow spectra, shown in Figure S2.

To understand the influence of the surface coverage of the HEL on ITO with respect to the device conductivity and performance, we investigated the morphologies of the samples with both SEM and AFM images. The SEM images of the bare ITO, ITO/CoO_x, ITO/PEDOT:PSS, ITO/NiO_x, and ITO/CuO_x films are illustrated in Figure 2a–d, respectively; the corresponding AFM surface topographies of the same samples are shown in Figure2e–h, respectively. The coverage of the HEL on the ITO surface is a critical factor to be considered to achieve a high performance of a device: If the HEL film is too thin and insufficiently rough, then it would be difficult to cover completely the ITO surface, which could lead to the $MAPbI_3$ layer in direct contact with ITO for current leakage to occur. If the HEL film is too thick and too rough, then the series resistance of the device becomes too large to provide satisfactory conductivity of the electrode. According to the AFM results, the root-mean-square roughness (R_{rms}) of bare ITO was 3.2 nm; the RMS roughness increased to 6.3 nm after being covered with a CoO_x layer. In contrast, the R_{rms} values of the NiO_x and CuO_x films are 4.2 and 3.9 nm, respectively, which are significantly smaller than that of the CoO_x film. On increasing the roughness of the HEL to some extent, the surface coverage can also be increased, according to preceding work.[43,44] A larger roughness of the CoO_x layer thus indicates that the surface coverage of this HEL on the ITO is greater

DOI: 10.1021/acsami.6b10803
ACS Appl. Mater. Interfaces 2016, 8, 33592–33600

than those of the others, which would result in conductivity of the CoO_x film being better than those of the other metal-oxide films.[45] In order to confirm the relation between the roughness of HELs and their conductivities, we have calculated the resistivity of each HELs using an electrochemical analyzer technique with a copper lead wire. The resistivities were calculated for the different HELs and founded to be 35.3, 50.2, and 56.5 Ω/cm for CoO_x, NiO_x, and CoO_x, respectively. Consequently, the conductivity of the corresponding samples found to be 0.030, 0.019, and 0.017 S/m, respectively. The roughness results (R_{rms}) were 6.3, 4.2, and 3.9 nm for CoO_x, NiO_x, and CuO_x, respectively. These results show good correlation with the obtained conductivity results. The complete experimental setup summarized is in the Experimental Section, and the box chart of the obtained results for the different HELs used in the current study are shown in Figure S3. Furthermore, the valence band maximum and the conduction band minimum of CoO_x were −5.2 and −2.3 eV, respectively.[46]

The perovskite layer was produced on top of the HEL with a combined FDC+SA method; its crystal morphology is shown in Figure 3a, displaying a full surface coverage of the perovskite crystals with grains of micrometer size. Furthermore, the crystal morphologies of perovskite layer on the other HELs, NiO_x and CuO_x, were studied according to the SEM images shown in Figure S4. We notice that there is no appreciable difference in the morphology of PSK on the different HELs. Figure 3b shows a typical cross-sectional SEM image of an inverted device with configuration glass/ITO/CoO_x/PSK/PCBM/Ag; the estimated thickness of each layer is indicated. It is noticed that the thickness of the HELs is very small which cannot be estimated from the SEM imaged precisely. Therefore, the X-ray reflectivity method was employed to check the thickness for each HEL. By comparing the obtained measured profile with a simulated one for each material, we can estimate the thickness of the thin films through fitting calculation. We used a model including HEL and ITO layers on the glass substrate, and the fitting parameters were thickness, roughness, and density of each layer.[47] The thickness of HELs were estimated to be 15, 10, and 17 nm for CoO_x, NiO_x, and CuO_x, respectively. To perceive the effect of HEL on the device performance, devices with the HEL made of PEDOT:PSS, NiO_x, and CuO_x were also fabricated according to the same experimental conditions for comparison. Figure 3c shows the current density−voltage (J−V) curves of devices of four types under AM 1.5 G 1 sun irradiation. The CoO_x device exhibits V_{OC} (V) = 0.949, J_{SC} (mA cm^{-2}) = 20.28, and fill factor (FF) = 0.755, corresponding to PCE = 14.5%, which is greater than that of devices assembled using the traditional HEL PEDOT:PSS (12.2%), and is significantly greater than those of the other two metal-oxide-based HEL, NiO_x (10.2%) and CuO_x (9.4%), under the same experimental conditions. The corresponding photovoltaic parameters of the four devices are summarized in Table 1. In order to confirm the continuity and uniformity of CoO_x layer, we have checked the device performance for the same cell at different positions. The results show good reproducibility as shown in Table S1. Furthermore, we have studied and checked 12 samples for cells with CoO_x as under-layer with the active area of 0.09 cm^2 in order to upscaling the perovskite solar cells. By comparing the obtained results of the smaller active area (0.02 cm^2) with the results of the upscaling PSCs with the active area (0.09 cm^2), we speculate that the efficiency decreases due to the series resistance. The results obtained from upscaling the PSCs with the active area of (0.09 cm^2) were shown and summarized in Figure S5 and Table S1, respectively.

Table 1. Photovoltaic Parameters of Inverted Planar Heterojunction Perovskite Solar Cells Fabricated with Varied p-Type HEL Materials

devices[a]	J_{SC} (mA cm^{-2})	V_{OC} (V)	FF	PCE (%)[b]
CoO_x	20.28	0.949	0.755	14.5[c] (12.4 ± 0.7)
PEDOT:PSS	18.80	0.879	0.740	12.2[c] (11.5 ± 0.7)
NiO_x	17.00	1.004	0.600	10.2[c] (9.3 ± 0.5)
CuO_x	16.10	0.915	0.639	9.4[c] (8.3 ± 0.4)

[a]The devices were fabricated using the hole-extraction layers (HELs) prepared via varied wet chemical methods detailed in the Experimental Section. [b]The average values shown in parentheses with the uncertainties representing one standard deviation were obtained from 30 devices fabricated under the same experimental conditions. [c]The best photovoltaic performances were obtained during the long-term stability examination.

In order to optimize the thickness of different HELs used in this study and their effect on the power conversion efficiency, we should check different thicknesses by changing the experimental parameters like spin-coating rate and time. For the planar perovskite solar cells, in order to obtain high power conversion efficiency, it is better to use an under-layer with small thickness. However, in case of the thickness less than 10 nm for all the HELs, it will be difficult to cover all the ITO area, and pin-holes will be found which will decrease the cells efficiency significantly. Therefore, we should use HELs with a thickness at least 10 or more.

In this study, we have prepared the under-layer metal oxides using a spin-coating rate of 6000 rpm for 50 s. For comparison and to optimize the thickness factor on PCE, we have checked the same under-layers with different spin-coating parameters (4000 rpm/30 s). As mentioned before, the thickness of HELs using standard spin-coating parameters of (6000 rpm/50 s) were estimated to be 15, 10, 17 nm for CoO_x, NiO_x, and CuO_x, respectively. By using the spin-coating thickness equation,[48] we can estimate the HELs thickness using spin-coating parameters of (4000 rpm/30 s) to be thicker by ∼30%. The estimated thickness of the HELs were 19, 13, and 22 nm for CoO_x, NiO_x, and CuO_x, respectively, using spin-coating parameters of (4000 rpm/30 s) determined by the X-ray reflectivity. Also, we obtained the power conversion efficiencies for every spin-coating parameter, and the PSCs using HELs with the slower spin-coating parameters (4000 rpm/30 s) showed poor photovoltaic performances than those with the faster spin-coating parameters (6000 rpm/50 s). The obtained results for 12 devices assembled using the different HELs with the slower spin-coating parameters of (4000 rpm/30 s) are shown in Figures S6−S8 and Tables S2−S4. Figure 3d shows IPCE action spectra of the corresponding devices with the integrated current densities, confirming the J_{SC} values with deviations within ∼10% between the two current density values. The J_{SC} value of the CoO_x device is significantly greater than those of the other devices because of the enhanced IPCE values in the visible region (550−700 nm) (Figure 3d). As mentioned in the IPCE results, there is an enhancement in the longer wavelength region in case of CoO_x compared to the other HELs. That may be due to the light-harvesting effect or the good charge separation. Furthermore, the absorption spectra of the perovskite films deposited on varied HEL are similar (Figure

DOI: 10.1021/acsami.6b10803
ACS Appl. Mater. Interfaces 2016, 8, 33592−33600

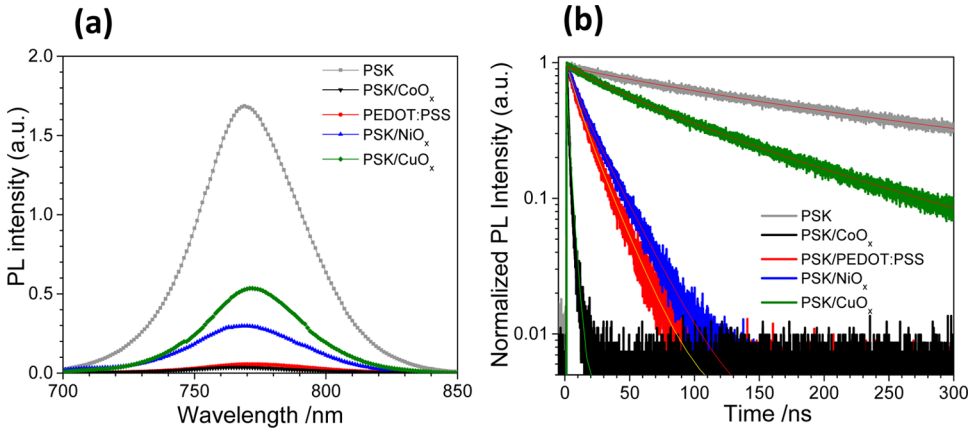

Figure 4. (a) Photoluminescence (PL) spectra and (b) PL decay profiles of $MAPbI_3$ (PSK), and PSK deposited on varied HEL films. The PL spectra were obtained at excitation wavelength 633 nm, and the transient PL decays were obtained using the TCSPC technique with excitation at 635 nm and probe at 770 nm.

S9), indicating that the enhancement in IPCE for the CoO_x device not from the light-harvesting effect but might be from the effect of charge separation. In contrast, the V_{OC} values show a systematic trend with order NiO_x (1.004 V) > CoO_x (0.949 V) > CuO_x (0.915 V) > PEDOT:PSS (0.879 V), which is consistent with the trend of their valence-band potential levels showing a reverse order: NiO_x (−5.4 eV) < CoO_x (−5.2 eV) < CuO_x (−5.1 eV) < PEDOT:PSS (−5.0 eV). The CoO_x device also exhibited the greatest FF value (0.755), indicating that a HEL of this type features less series resistance than of the other devices. The greater J_{SC} and FF values for the CoO_x device might be attributed to the hole-extraction ability, which is greater for the CoO_x layer than those for the other HEL materials; this effect is further examined below.

To gain further insight into the charge-extraction property of the HEL films affecting their corresponding photovoltaic performances, we undertook time-resolved spectral measurements for perovskite deposited on varied HEL films investigated herein. First, we performed steady-state photoluminescence (PL) measurements to assess the effect of PL quenching of perovskite due to varied charge extraction of those PSK/HEL films. As the PL spectra show in Figure 4a, the PL intensity of PSK decreased significantly when the PSK layer was in contact with the HEL showing PL intensities with order CuO_x > NiO_x > PEDOT:PSS > CoO_x, indicating the hole-extracting ability in the reverse order, i.e., the CoO_x film should have the best hole-extracting ability due to the existence of an efficient nonradiative process to quench the PL effectively. To investigate further the kinetics of this efficient nonradiative process, we measured transient PL decay using the time-correlated single-photon-counting (TCSPC) technique with excitation at 635 nm and probe at 770 nm. The PL transient profiles shown in Figure 4b are well fitted with a biexponential decay function; the fitted time coefficients (τ_i) for each sample are shown in Table 2 with the corresponding relative amplitudes (A_i) shown in parentheses. The average PL lifetimes (τ_{PL}) were determined with an intensity-averaged approach reported elsewhere.[49] τ_{PL} for only $MAPbI_3$ deposited on ITO was determined to be 369.6 ns but decreased to 2.8, 16.8, 21.6, and 136.7 ns when perovskite was in contact with the HEL of CoO_x, PEDOT:PSS, NiO_x, and CuO_x, respectively. Assuming that hole extraction by the HEL is the most predominant nonradiative relaxation path, the interfacial hole extraction times (τ_h) in the $MAPbI_3$/HTM interface can be estimated to

Table 2. Photoluminescence (PL) Decay Time Coefficientsof Perovskite (PSK) Deposited on Varied *p*-type Hole-Extraction Layers with Excitation at 635 nm and Probed at 770 nm

films	τ_1 (ns) (A_1)[a]	τ_2 (ns) (A_2)[a]	τ_{PL}(ns)[b]	τ_h (ns)[c]
PSK	124.3 (0.39)	445.5 (0.61)	396.9	
PSK/CoO_x	2.8 (1)		2.8	2.8
PSK/PEDOT:PSS	7.4 (0.35)	18.8 (0.65)	16.8	17.5
PSK/NiO_x	9.2 (0.30)	23.7 (0.70)	21.6	22.8
PSK/CuO_x	55.4 (0.45)	159.8 (0.55)	136.7	208.5

[a]Relative amplitudes shown in parentheses. [b]The average PL lifetimes were determined according to the following equation,

$$\tau_{PL} = \frac{\sum A_i \tau_i^2}{\sum A_i \tau_i}$$

in which τ_i and A_i are the fitted time coefficients and the corresponding amplitudes of each component, respectively. [c]The interfacial hole-extraction time (τ_h) at the interface between PSK and HEL can be predicted using the following equation

$$\frac{1}{\tau_h} = \frac{1}{\tau_{PSK/HEL}} - \frac{1}{\tau_{PSK}}$$

in which τ_{PSK} and $\tau_{PSK/HEL}$ are the PL lifetimes for PSK only and those with PSK deposited on varied HEL films, respectively.

be 2.8, 17.5, 22.8, and 208.5 ns for HEL of CoO_x, PEDOT:PSS, NiO_x, and CuO_x, respectively; details of the determination of τ_{PL} and τ_h appear in the footnote of Table 2. Our results indicate that the hole-extraction time of the CoO_x layer is much shorter than those of the other HEL, which reasonably explains the superior photovoltaic performance of the CoO_x device with greater J_{SC} and FF values than those of other devices.

The performance reproducibility of the devices was examined on fabricating 30 identical devices according to the same experimental procedure for each HEL film; the corresponding photovoltaic parameters for the CoO_x, PEDOT:PSS, NiO_x, and CuO_x devices are summarized in Tables S5−S8, respectively. Figure 5a shows histograms of the PCE distributions for devices made of these four HEL for comparison; the corresponding histograms for the other photovoltaic parameters are shown in Figure S10. Our results show that these devices were satisfactorily reproducible with average PCE (%) = 12.4 ±

DOI: 10.1021/acsami.6b10803
ACS Appl. Mater. Interfaces 2016, 8, 33592−33600

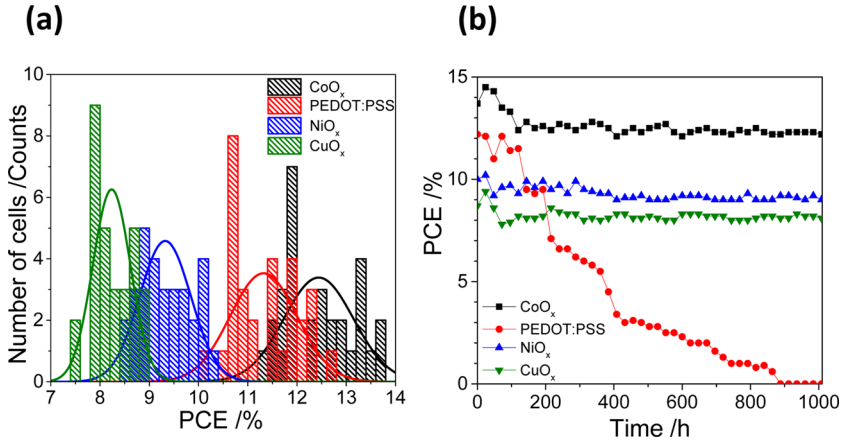

Figure 5. (a) PCE distribution histograms and (b) PCE vs storage period for devices with HEL made of CoO_x, PEDOT:PSS, NiO_x, and CuO_x as indicated.

0.7, 11.5 ± 0.7, 9.3 ± 0.5, and 8.3 ± 0.4 for devices made of CoO_x, PEDOT:PSS, NiO_x, and CuO_x, respectively; these average values are shown in parentheses in Table 1. To examine their long-term stability, we tested also the endurance of the devices of the four types kept in darkness and in glovebox under a N_2 atmosphere; the corresponding stability results are shown in Figure 5b. Even though the performance of the PEDOT:PSS device retained PCE ≈ 12% in the first 100 h, it degraded rapidly after 100 h; the efficiency vanished after storage over 900 h. In contrast, all devices made of metal-oxide HEL (CoO_x, NiO_x, and CuO_x) demonstrated great enduring stability over a period 43 days (more than 1000 h) and maintained ~90% of their initial efficiencies with the trend of performance showing the order CoO_x > NiO_x > CuO_x. The rapid degradation of the PEDOT:PSS device might be due to the acidic and hygroscopic characteristics of the polymer that damage the ITO electrode as well as the adjacent moisture-sensitive $MAPbI_3$ layer.[50,51] Our results thus indicate not only the great device performance but also the excellent enduring stability of the CoO_x device as a promising candidate for future photovoltaic applications.

CONCLUSIONS

A simple solution method was used to prepare a uniform and ultrathin layer of CoO_x as an efficient HEL electrode for inverted planar heterojunction perovskite solar cells. The prepared CoO_x film has an effective surface coverage to avoid contact between the perovskite layer and the ITO substrate; it also features sufficient surface roughness to provide an intimate junction of large interfacial area to form a uniform perovskite layer with effective hole-extracting characteristics. When the PHJ devices were fabricated with CoO_x as HEL, the best photovoltaic performance attained PCE 14.5%, which is superior to those of the devices with the HEL made of PEDOT:PSS, NiO_x, and CuO_x under the same experimental conditions. The results of measurements of steady-state and time-resolved photoluminescence show hole-extraction rates with order CoO_x > PEDOT:PSS > NiO_x > CuO_x, which is consistent with the trend of their corresponding photovoltaic performances in the same order. The origin of the high performance of the CoO_x device is rationalized to be its great hole-extraction ability at the $MAPbI_3/CoO_x$ interface with decreased interfacial charge recombination. Thirty devices of each type of HEL were fabricated to examine the reproducibility of the performance with the average PCE showing the same order. Tests of enduring stability in performance in air showed the outstanding long-term stability of devices made of metal-oxide HEL, with the best CoO_x cell retaining 90% of its initial performance after storage period 1000 h. The ultrathin CoO_x HEL is thus a promising alternative as a p-type electrode for inverted planar perovskite solar cells with the advantages of high performance, low cost, ease of processing, and great stability for future commercialization.

EXPERIMENTAL METHODS

Preparation of Metal-Oxide Precursor Solutions. The precursor of the CoO_x film was prepared with cobalt acetate tetrahydrate (Alfa Aesar, 0.5 M) in ethandiol solution containing 1,2-diaminoethane (Aldrich, 1 M) stirred for at least 3 days to form a homogeneous precursor solution that was then filtered with nylon filters (0.45 mm).[52] NiO_x and CuO_x solutions were prepared with the same method for comparison; copper sulfate pentahydrate and nickel formate dihydrate were precursors for CuO_x and NiO_x, respectively.[53,54]

Preparation of Perovskite Precursor Solution. Methylammonium iodide (CH_3NH_3I) was synthesized via the reaction of methylamine (CH_3NH_2, 21.6 mL, 40 mass % in water, Alfa Aesar) and hydriodic acid (HI, 30 mL, 57 mass % in water, with hypophosphorous acid 1.5%, Alfa Aesar) and kept stirred at 0 °C for 2 h under a N_2 atmosphere, followed by rotary evaporation to remove the solvent. The CH_3NH_3I powder was washed three times with diethyl ether (99%, anhydrous, ECHO) and dried in a vacuum oven at 50 °C overnight before use. CH_3NH_3I was synthesized as described elsewhere.[55,56] $MAPbI_3$ precursor solutions (concentration 45% by mass) were prepared in *N*,*N*-dimethylformamide (DMF, anhydrous, Aldrich, 1 mL) mixed with powdered CH_3NH_3I (175 mg) and PbI_2 (99%, Aldrich, 507 mg). The solution was stirred at 70 °C for 1 h before use.

Fabrication of Electrodes and Devices. Indium-doped tin oxide (ITO) (TEC7, Hartford, USA) was partially removed from the substrate via etching with zinc powder and HCl (2 M) to produce the desired pattern. The patterned ITO substrates were cleaned with ultrasonication for 30 min in a mixture (acetone, soapy water and isopropyl alcohol (IPA), 1:1:1) and then washed with deionized water. Afterward, the glass was dried with a N_2 blow gun. The CoO_x, PEDOT:PSS, NiO_x, and CuO_x films were deposited on ITO in the same way via spin-coating of the solution (50 μL, 6000 rpm, 50 s) and annealed at 300 °C for 2 h in a N_2 atmosphere, then annealed at 400 °C for 1 h in air, except for the PEDOT:PSS samples prepared without further annealing. The substrates were subsequently exposed to ozone for 18 min via irradiation (excimer lamp PC-01-H, N-Cobo Co.) under an O_2 atmosphere to remove the organic residues. The prepared

DOI: 10.1021/acsami.6b10803
ACS Appl. Mater. Interfaces 2016, 8, 33592−33600

$MAPbI_3$ precursor solution was deposited onto the HEL/ITO substrate with spin-coating at 5000 rpm for 15 s; a few drops of chlorobenzene (CBZ) as antisolvent were dripped onto the substrate during spin-coating after a delay (5 s). The $MAPbI_3$-precursor coated substrates were then dried on a hot plate at 100 °C for 10 min using solvent annealing (SA) with DMF drop (5 μL). The phenyl-C_{61}-butanoic acid methyl ester (PCBM, Uni Region Bio-Tech, Taiwan) layer was subsequently deposited with spin-coating (18 mg mL^{-1} in CBZ as solvent) at 1000 rpm for 30 s. The device was eventually completed with the thermal evaporation of Ag contact electrodes (100 nm) in a high vacuum through a shadow mask; the active area of the Ag electrodes in the fabricated device was 0.02 cm^2. The same procedure was applied for the other HEL (PEDOT:PSS, NiO_x, and CuO_x) for comparison.

Structure and Surface Measurements. The crystalline phases were identified with X-ray diffraction (XRD) (RINT-2000/PC RIGAKU, Cu Kα radiation, scanning speed 2° (2θ)/min within 2θ range 5−60°). The particle morphology and structure were examined with a field-emission scanning electron microscope (FESEM, Hitachi SU8010, maximum resolution 1 nm at electron acceleration voltage 15 kV) and an atomic force microscope (AFM, Nanoscale hybrid microscope VN-8010, Keyence microscope, Japan). The UV−visible absorption spectra were recorded with a spectrometer (JASCO V-570). To analyze the chemical composition of the surfaces we used an X-ray photoemission spectrometer (JPS-9200, JEOL) to record the X-ray photoemission spectrum (XPS). The Al Kα line served as the X-ray source; the C 1s signal served as an internal reference (284.6 eV).

Photovoltaic and PL Lifetime Measurements. The $J-V$ curves were measured with a digital source meter (Keithley 2400) under 1 sun illumination (AM 1.5 G, 100 mW cm^{-2}) from a solar simulator (XES-40S1, SAN-E1). The IPCE spectra were recorded with a system comprising a Xe lamp (A-1010, PTi, 150 W) and monochromator (PTi, 1200 groove mm^{-1} blazed at 500 nm). Photoluminescence (PL) transients were recorded with a time-correlated single-photon-counting (TCSPC) system (Fluotime200, PicoQuant) with excitation at 635 nm from a picosecond pulsed-diode laser (LDH-635, PicoQuant, fwhm ∼70 ps); the PL temporal profiles were collected at 770 nm.

Conductivity and Thickness Measurements. The conductivity was calculated using an electrochemical analyzer (ALS/CH Instruments 852C, ALS) technique with a copper lead wire. The experimental setup of the measurements is as follows: Two electrodes of the electrochemical analyzer are connected to the sample: one to the ITO part and the other to the HELs surface. We have checked the resistivity at different positions on the HEL surface. Almost 15 positions have been checked for each sample and get the mean of them. The distance between the two electrodes was stable at all the measurements for CoO_x HEL and also fixed for the other HELs in order to make the comparison between all of them more precise. The HELs thickness were estimated using X-ray reflectivity by Bruker D8 discover instrument, with X-ray source of Cu Kα (45 kV, 360 mA), divergence slit: 0.05 mm, scattering slit: 0.1 mm, and receiving slit: 0.1 mm.

■ ASSOCIATED CONTENT

Supporting Information

The Supporting Information is available free of charge on the ACS Publications website at DOI: 10.1021/acsami.6b10803.

XRD patterns of the $MAPbI_3$ layer and CoO_x, NiO_x, and CuO_x films deposited on an ITO substrate as well as PSK on the different HELs, XPS elemental analysis of CoO_x, NiO_x, and CuO_x films in detail, box chart for the obtained resistivity results for the different HELs, top-view SEM image of perovskite on NiO_x and CuO_x, results of 12 devices for upscaling the CoO_x PSCs with active area (0.09 cm^2), absorption spectra of PSK on the different HELs, results of optimization the thickness, photovoltaic performance histograms of 30 devices made of HEL of four types, and tables summarizing the corresponding photovoltaic parameters. (PDF)

■ AUTHOR INFORMATION

Corresponding Authors

*E-mail:diau@mail.nctu.edu.tw.

*E-mail:misawa@es.hokudai.ac.jp.

ORCID

Hiroaki Misawa: 0000-0003-1070-387X

Notes

The authors declare no competing financial interest.

■ ACKNOWLEDGMENTS

Funds from Ministry of Education, Culture, Sports, Science and Technology of Japan (KAKENHI grant numbers JP23225006 and JP15H00856, AnApple), Nanotechnology Platform (Hokkaido University) and Dynamic Alliance for Open Innovation Bridging Human, Environment and Materials (Five-Star Alliance) of MEXT, Taiwan Ministry of Science and Technology (contracts MOST 105-2119-M-009-011-MY3 and MOST 104-2119-M-009-001) supported this research. A.E.S. thanks National Chiao Tung University (Hsinchu, Taiwan) and Hokkaido University (Sapporo, Japan) for support of his visit to NCTU through the Elite Internship Program agreement between the two universities.

■ REFERENCES

(1) Green, M. A.; Ho-Baillie, A.; Snaith, H. J. The Emergence of Perovskite Solar Cells. *Nat. Photonics* **2014**, *8*, 506−514.

(2) Xing, G.; Mathews, N.; Lim, S. S.; Yantara, N.; Liu, X.; Sabba, D.; Grätzel, M.; Mhaisalkar, S.; Sum, T. C. Low-Temperature Solution-Processed Wavelength-Tunable Perovskites for Lasing. *Nat. Mater.* **2014**, *13*, 476−480.

(3) Lee, M. M.; Teuscher, J.; Miyasaka, T.; Murakami, T. N.; Snaith, H. J. Efficient Hybrid Solar Cells Based on Meso-Superstructured Organometal Halide Perovskites. *Science* **2012**, *338*, 643−647.

(4) De Wolf, S.; Holovsky, J.; Moon, S. J.; Löper, P.; Niesen, B.; Ledinsky, M.; Haug, F. J.; Yum, J. H.; Ballif, C. Organometallic Halide Perovskites: Sharp Optical Absorption Edge and Its Relation to Photovoltaic Performance. *J. Phys. Chem. Lett.* **2014**, *5*, 1035−1039.

(5) Takahashi, Y.; Hasegawa, H.; Takahashi, Y.; Inabe, T. Hall Mobility in Tin Iodide Perovskite $CH_3NH_3SnI_3$: Evidence for a Doped Semiconductor. *J. Solid State Chem.* **2013**, *205*, 39−43.

(6) Wehrenfennig, C.; Eperon, G. E.; Johnston, M. B.; Snaith, H. J.; Herz, L. M. High Charge Carrier Mobilities and Lifetimes in Organolead Trihalide Perovskites. *Adv. Mater.* **2014**, *26*, 1584−1589.

(7) Yin, W.-J.; Shi, T.; Yan, Y. Unusual Defect Physics in $CH_3NH_3PbI_3$ Perovskite Solar Cell Absorber. *Appl. Phys. Lett.* **2014**, *104*, 063903.

(8) Kojima, A.; Teshima, K.; Shirai, Y.; Miyasaka, T. Organometal Halide Perovskites as Visible-light Sensitizers for Photovoltaic Cells. *J. Am. Chem. Soc.* **2009**, *131*, 6050−6051.

(9) Jeon, N. J.; Noh, J. H.; Yang, W. S.; Kim, Y. C.; Ryu, S.; Seo, J.; Seok, S. I. Compositional Engineering of Perovskite Materials for High-Performance Solar Cells. *Nature* **2015**, *517*, 476−480.

(10) Zhou, H.; Chen, Q.; Li, G.; Luo, S.; Song, T. B.; Duan, H. S.; Hong, Z.; You, J.; Liu, Y.; Yang, Y. Photovoltaics. Interface Engineering of Highly Efficient Perovskite Solar Cells. *Science* **2014**, *345*, 542−546.

(11) Xue, Q. F.; Sun, C.; Hu, Z. C.; Huang, F.; Yip, H.-L.; Cao, Y. Recent Advances in Perovskite Solar Cells: Morphology Control and Interfacial Engineering. *Huaxue Xuebao* **2015**, *73*, 179−192.

(12) Nie, W.; Tsai, H.; Asadpour, R.; Blancon, J. C.; Neukirch, A. J.; Gupta, G.; Crochet, J. J.; Chhowalla, M.; Tretiak, S.; Alam, M. A.; Wang, H. L.; Mohite, A. D. Solar Cells. High-Efficiency Solution-

DOI: 10.1021/acsami.6b10803
ACS Appl. Mater. Interfaces 2016, 8, 33592−33600

processed Perovskite Solar Cells with Millimeter-scale Grains. *Science* **2015**, *347*, 522−525.
(13) Liang, P. W.; Liao, C. Y.; Chueh, C. C.; Zuo, F.; Williams, S. T.; Xin, X.-K.; Lin, J.; Jen, A. K.-Y. Additive Enhanced Crystallization of Solution-Processed Perovskite for Highly Efficient Planar-Heterojunction Solar Cells. *Adv. Mater.* **2014**, *26*, 3748−3754.
(14) Heo, J. H.; Song, D. H.; Han, H. J.; Kim, S. Y.; Kim, J. H.; Kim, D.; Shin, H. W.; Ahn, T. K.; Wolf, C.; Lee, T.-W.; Im, S. H. Planar $CH_3NH_3PbI_3$ Perovskite Solar Cells with Constant 17.2% Average Power Conversion Efficiency Irrespective of the Scan Rate. *Adv. Mater.* **2015**, *27*, 3424−3430.
(15) Wu, C. G.; Chiang, C. H.; Tseng, Z. L.; Nazeeruddin, Md. K.; Hagfeldt, A.; Grätzel, M. High Efficiency Stable Inverted Perovskite Solar Cells Without Current Hysteresis. *Energy Environ. Sci.* **2015**, *8*, 2725−2733.
(16) Heo, J. H.; Han, H. J.; Kim, D.; Ahn, T. K.; Im, S. H. Hysteresis-less Inverted $CH_3NH_3PbI_3$ Planar Perovskite Hybrid Solar Cells with 18.1% Power Conversion Efficiency. *Energy Environ. Sci.* **2015**, *8*, 1602−1608.
(17) Chen, W.; Wu, Y. Z.; Yue, Y. F.; Liu, J.; Zhang, W.; Yang, X.; Chen, H.; Bi, E.; Ashraful, I.; Grätzel, M.; Han, L. Efficient and Stable Large-area Perovskite Solar Cells with Inorganic Charge Extraction Layers. *Science* **2015**, *350*, 944−948.
(18) Chiang, C. H.; Tseng, Z. L.; Wu, C. G. Planar Heterojunction Perovskite/$PC_{71}BM$ Solar Cells with Enhanced Open-circuit Voltage *via* a (2/1)-step Spin-coating Process. *J. Mater. Chem. A* **2014**, *2*, 15897−15903.
(19) Jasieniak, J. J.; Seifter, J.; Jo, J.; Mates, T.; Heeger, A. J. A Solution-processed MoO_x Anode Interlayer for Use within Organic Photovoltaic Devices. *Adv. Funct. Mater.* **2012**, *22*, 2594−2605.
(20) Yan, W.; Ye, S.; Li, Y.; Sun, W.; Rao, H.; Liu, Z.; Bian, Z.; Huang, C. Hole-Transporting Materials in Inverted Planar Perovskite Solar Cells. *Adv. Energy Mater.* **2016**, *6*, 1600474.
(21) Ratcliff, E. L.; Meyer, J.; Steirer, K. X.; Garcia, A.; Berry, J. J.; Ginley, D. S.; Olson, D. C.; Kahn, A.; Armstrong, N. R. Evidence for Near-Surface NiOOH Species in Solution-Processed NiO_x Selective Interlayer Materials: Impact on Energetics and the Performance of Polymer Bulk Heterojunction Photovoltaics. *Chem. Mater.* **2011**, *23*, 4988−5000.
(22) Yu, Z.-K.; Fu, W.-F.; Liu, W.-Q.; Zhang, Z.-Q.; Liu, Y.-J.; Yan, J.-L.; Ye, T.; Yang, W.-T.; Li, H.-Y.; Chen, H.-Z. Solution-processed CuO_x as an Efficient Hole-extraction Layer for Inverted Planar Heterojunction Perovskite Solar Cells. *Chin. Chem. Lett.* **2016**, DOI: 10.1016/j.cclet.2016.06.021.
(23) Subbiah, A. S.; Halder, A.; Ghosh, S.; Mahuli, N.; Hodes, G.; Sarkar, S. K. Inorganic Hole Conducting Layers for Perovskite-based Solar Cells. *J. Phys. Chem. Lett.* **2014**, *5*, 1748−1753.
(24) Kim, J. H.; Liang, P.-W.; Williams, S. T.; Cho, N.; Chueh, C. C.; Glaz, M. S.; Ginger, D. S.; Jen, A. K.-Y. High-performance and Environmentally Stable Planar Heterojunction Perovskite Solar cells Based on a Solution-processed Copper-doped Nickel-oxide Hole-transporting Layer. *Adv. Mater.* **2015**, *27*, 695−701.
(25) Chatterjee, S.; Pal, A. J. Introducing Cu_2O Thin Films as a Hole-Transport Layer in Efficient Planar Perovskite Solar Cell Structures. *J. Phys. Chem. C* **2016**, *120*, 1428−1437.
(26) Rao, H.; Ye, S.; Sun, W.; Yan, W.; Li, Y.; Peng, H.; Liu, Z.; Bian, Z.; Li, Y.; Huang, C. A 19.0% Efficiency Achieved in CuO_x-based Inverted $CH_3NH_3PbI_{3-x}Cl_x$ Solar Cells by an Effective Cl Doping Method. *Nano Energy* **2016**, *27*, 51−57.
(27) Ye, S.; Sun, W.; Li, Y.; Yan, W.; Peng, H.; Bian, Z.; Liu, Z.; Huang, C. CuSCN-based Inverted Planar Perovskite Solar Cell with an Average PCE of 15.6%. *Nano Lett.* **2015**, *15*, 3723−3728.
(28) Qin, P.; Tanaka, S.; Ito, S.; Tetreault, N.; Manabe, K.; Nishino, H.; Nazeeruddin, M. K.; Grätzel, M. Inorganic Hole Conductor-based Lead Halide Perovskite Solar Cells with 12.4% Conversion Efficiency. *Nat. Commun.* **2014**, *5*, 3834.
(29) Meyer, J.; Hamwi, S.; Kröger, M.; Kowalsky, W.; Riedl, T.; Kahn, A. Transition Metal Oxides for Organic Electronics: Energetics, Device Physics and Applications. *Adv. Mater.* **2012**, *24*, 5408−5427.
(30) Zhao, Y.; Nardes, A. M.; Zhu, K. Effective Hole Extraction Using MoO_x-Al Contact in Perovskite $CH_3NH_3PbI_3$ Solar Cells. *Appl. Phys. Lett.* **2014**, *104*, 213906.
(31) Jeng, J. Y.; Chen, K. C.; Chiang, T. Y.; Lin, P. Y.; Tsai, T. D.; Chang, Y. C.; Guo, T. F.; Chen, P.; Wen, T. C.; Hsu, Y. J. Nickel Oxide Electrode Interlayer in $CH_3NH_3PbI_3$ Perovskite/PCBM Planar-Heterojunction Hybrid Solar Cells. *Adv. Mater.* **2014**, *26*, 4107−4113.
(32) Xiao, M.; Huang, F.; Huang, W.; Dkhissi, Y.; Zhu, Y.; Etheridge, J.; Gray-Weale, A.; Bach, U.; Cheng, Y.-B.; Spiccia, L. A Fast Deposition-Crystallization Procedure for Highly Efficient Lead Iodide Perovskite Thin-Film Solar Cells. *Angew. Chem., Int. Ed.* **2014**, *53*, 9898−9903.
(33) Xiao, Z.; Dong, Q.; Bi, C.; Shao, Y.; Yuan, Y.; Huang, J. Solvent Annealing of Perovskite-Induced Crystal Growth for Photovoltaic-Device Efficiency Enhancement. *Adv. Mater.* **2014**, *26*, 6503−6509.
(34) Chiang, C.-H.; Wu, C.-G. Bulk Heterojunction Perovskite−PCBM Solar Cells with High Fill Factor. *Nat. Photonics* **2016**, *10*, 196−200.
(35) Mao, Y.-Q.; Zhou, Z.-J.; Ling, T.; Du, X.-W. P-type CoO Nanowire Arrays and Their Application in Quantum Dot-sensitized Solar Cells. *RSC Adv.* **2013**, *3*, 1217−1221.
(36) Endres, J.; Egger, D. A.; Kulbak, M.; Kerner, R. A.; Zhao, L.; Silver, S. H.; Hodes, G.; Rand, B. P.; Cahen, D.; Kronik, L.; Kahn, A. Valence and Conduction Band Densities of States of Metal Halide Perovskites: A Combined Experimental−Theoretical Study. *J. Phys. Chem. Lett.* **2016**, *7*, 2722−2729.
(37) Subbiah, A. S.; Halder, A.; Ghosh, S.; Mahuli, N.; Hodes, G.; Sarkar, S. K. Inorganic Hole Conducting Layers for Perovskite-based Solar Cells. *J. Phys. Chem. Lett.* **2014**, *5*, 1748−1753.
(38) Gulino, A.; Fiorito, G.; Fragalà, I. Deposition of Thin Films of Cobalt Oxides by MOCVD. *J. Mater. Chem.* **2003**, *13*, 861−865.
(39) Buono-Core, G. E.; Tejos, M.; Schrebler, R.; Klahn, A. H.; Hill, R. H. Nickel Tropolonate Complexes as Precursors for the Direct Photodeposition of NiO Thin Films. *J. Chil. Chem. Soc.* **2004**, *49*, 223−226.
(40) Remédios, C. M. R.; Sasaki, J. M. Formation Studies of NiO by X-ray Powder Diffraction. *Powder Diffr.* **2008**, *23* (S1), 56−58.
(41) Cheng, S.-L.; Chen, M. F. Fabrication, Characterization, and Kinetic Study of Vertical Single-Crystalline CuO Nanowires on Si Substrates. *Nanoscale Res. Lett.* **2012**, *7*, 119−126.
(42) Liang, K.; Mitzi, D. B.; Prikas, M. T. Synthesis and Characterization of Organic−Inorganic Perovskite Thin Films Prepared Using a Versatile Two-Step Dipping Technique. *Chem. Mater.* **1998**, *10*, 403−411.
(43) Pons, L.; Délia, M.-L.; Bergel, A. Effect of Surface Roughness, Biofilm Coverage and Biofilm Structure on the Electrochemical Efficiency of Microbial Cathodes. *Bioresour. Technol.* **2011**, *102*, 2678−2683.
(44) Malinkiewicz, O.; Roldan-Carmona, C.; Soriano, A.; Bandiello, E.; Camacho, L.; Nazeeruddin, M. K.; Bolink, H. J. Metal-Oxide-Free Methylammonium Lead Iodide Perovskite-based Solar Cells: the Influence of Organic Charge Transport Layers. *Adv. Energy Mater.* **2014**, *4*, 1400345.
(45) Ketenoğlu, D.; Ünal, B. Influence of Surface Roughness on the Electrical Conductivity of Semiconducting Thin Films. *Phys. A (Amsterdam, Neth.)* **2013**, *392*, 3008−3017.
(46) Das, S.; Coulter, J. E.; Manousakis, E. Convergence of Quasiparticle Self-Consistent GW Calculations of Transition-Metal Monoxides. *Phys. Rev. B: Condens. Matter Mater. Phys.* **2015**, *91*, 115105.
(47) Funahashi, M.; Kuraoka, M.; Fujimura, S.; Kobayashi, H.; Kohno, H.; Wilson, R. BST Thin Film Evaluation Using X-Ray Fluorescence and Reflectivity Methods. *Adv. X-Ray Anal.* **2000**, *42*, 109−118.
(48) Tyona, M. D. A Theoritical Study on Spin Coating Technique. *Advances in Materials Research* **2013**, *2*, 195−208.
(49) Valeur, B. Molecular Fluorescence. In *Encyclopedia of Applied Physics*; Stock, R., Ed.; Wiley-VCH Verlag GmbH & Co. KGaA: Weinheim, 2009.

DOI: 10.1021/acsami.6b10803
ACS Appl. Mater. Interfaces 2016, 8, 33592−33600

(50) Zhang, H.; Cheng, J.; Lin, F.; He, H.; Mao, J.; Wong, K. S.; Jen, A. K.-Y.; Choy, W. C. H. Pinhole-Free and Surface-Nanostructured NiO_x Film by Room-Temperature Solution Process for High-Performance Flexible Perovskite Solar Cells with Good Stability and Reproducibility. *ACS Nano* **2016**, *10*, 1503−1511.
(51) Berhe, T. A.; Su, W.-N.; Chen, C.-H.; Pan, C.-J.; Cheng, J.-H.; Chen, H.-M.; Tsai, M.-C.; Chen, L.-Y.; Dubale, A. A.; Hwang, B.-J. Organometal Halide Perovskite Solar Cells: Degradation and Stability. *Energy Environ. Sci.* **2016**, *9*, 323−356.
(52) Garcia, A.; Welch, G. C.; Ratcliff, E. L.; Ginley, D. S.; Bazan, G. C.; Olson, D. C. Improvement of Interfacial Contacts for New Small-Molecule Bulk-Heterojunction Organic Photovoltaics. *Adv. Mater.* **2012**, *24*, 5368−5373.
(53) Wang, K. C.; Jeng, J. Y.; Shen, P. S.; Chang, Y. C.; Diau, E. W.; Tsai, C. H.; Chao, T. Y.; Hsu, H. C.; Lin, P. Y.; Chen, P.; Guo, T. F.; Wen, T. C. P-type Mesoscopic Nickel Oxide/Organometallic Perovskite Heterojunction Solar Cells. *Sci. Rep.* **2014**, *4*, 4756.
(54) Gawande, M. B.; Goswami, A.; Felpin, F.-X.; Asefa, T.; Huang, X.; Silva, R.; Zou, X.; Zboril, R.; Varma, R. S. Cu and Cu-based Nanoparticles: Synthesis and Applications in Catalysis. *Chem. Rev.* **2016**, *116*, 3722−3811.
(55) Chan, C.-Y.; Wang, Y.; Wu, G.-W.; Diau, E. W.-G. Solvent-extraction Crystal Growth for Highly Efficient Carbon-based Mesoscopic Perovskite Solar Cells Free of Hole Conductors. *J. Mater. Chem. A* **2016**, *4*, 3872−3878.
(56) Chung, C.-C.; Lee, C. S.; Jokar, E.; Kim, J. H.; Diau, E. W.-G. Well-organized Mesoporous TiO_2 Photoanode Using Amphiphilic Graft Copolymer for Efficient Perovskite Solar Cells. *J. Phys. Chem. C* **2016**, *120*, 9619−9627.
(57) Mali, S. S.; Hong, C. K. p-i-n/n-i-p Type Planar Hybrid Structure of Highly Efficient Perovskite Solar Cells towards Improved Air Stability: Synthetic Strategies and the Role of p-type Hole Transport Layer (HTL) and n-type Electron Transport Layer (ETL) Metal Oxides. *Nanoscale* **2016**, *8*, 10528−10540.
(58) Song, Y.; Lv, S.; Liu, X.; Li, X.; Wang, S.; Wei, H.; Li, D.; Xiao, Y.; Meng, Q. Energy Level Tuning of TPB-based Hole-Transporting Materials for Highly Efficient Perovskite Solar Cells. *Chem. Commun.* **2014**, *50*, 15239−15242.
(59) Steck, C.; Franckevičius, M.; Zakeeruddin, S. M.; Mishra, A.; Bäuerle, P.; Grätzel, M. A−D−A-type *S,N*-Heteropentacene-based Hole Transport Materials for Dopant-Free Perovskite Solar Cells. *J. Mater. Chem. A* **2015**, *3*, 17738−17746.

DOI: 10.1021/acsami.6b10803
ACS Appl. Mater. Interfaces 2016, 8, 33592−33600